Neuro-Oncology

Improved detection of diffuse glioma infiltration with imaging combinations: a diagnostic accuracy study

Niels Verburg, Thomas Koopman, Maqsood M. Yaqub, Otto S. Hoekstra, Adriaan A. Lammertsma, Frederik Barkhof, Petra J. W. Pouwels, Jaap C. Reijneveld, Jan J. Heimans, Annemarie J. M. Rozemuller, Anne M. E. Bruynzeel, Frank Lagerwaard, William P. Vandertop, Ronald Boellaard, Pieter Wesseling, and Philip C. de Witt Hamer

Brain Tumor Center Amsterdam, Amsterdam University Medical Center (UMC), Amsterdam, Netherlands (N.V., J.C.R., W.P.V., P.W., P.C.W.H.), Neurosurgical Center Amsterdam, Amsterdam UMC, Amsterdam, Netherlands (N.V., W.P.V., P.W., P.C.W.H.); Department of Radiology and Nuclear Medicine, Amsterdam UMC, location Free University Medical Center (VUmc), Amsterdam, Netherlands (T.K., M.M.Y., O.S.H., A.A.L., F.B., P.J.W.P., R.B.); University College London Institute of Neurology and Healthcare Engineering, London, UK (F.B.); Department of Neurology, Amsterdam UMC, VUmc, Amsterdam, Netherlands (J.C.R., J.J.H.); Department of Pathology, Amsterdam UMC, VUmc, Amsterdam, Netherlands (A.J.M.R., P.W.), Department of Radiotherapy, Amsterdam UMC, VUmc, Amsterdam, Netherlands (A.M.E.B., F.L.); Princess Máxima Center for Pediatric Oncology and Department of Pathology, UMC Utrecht, Utrecht, Netherlands (P.W.)

Corresponding Author: Philip de Witt Hamer, MD PhD, Neurosurgeon, Department of Neurosurgery, Amsterdam UMC, location VUmc, De Boelelaan 1117, 1081 HV Amsterdam, The Netherlands (p.dewitthamer@vumc.nl).

Abstract

Background. Surgical resection and irradiation of diffuse glioma are guided by standard MRI: T2/fluid attenuated inversion recovery (FLAIR)–weighted MRI for non-enhancing and T1-weighted gadolinium-enhanced (T1G) MRI for enhancing gliomas. Amino acid PET has been suggested as the new standard. Imaging combinations may improve standard MRI and amino acid PET. The aim of the study was to determine the accuracy of imaging combinations to detect glioma infiltration.
Methods. We included 20 consecutive adults with newly diagnosed non-enhancing glioma (7 diffuse astrocytomas, isocitrate dehydrogenase [IDH] mutant; 1 oligodendroglioma, IDH mutant and 1p/19q codeleted; 1 glioblastoma IDH wildtype) or enhancing glioma (glioblastoma, 9 IDH wildtype and 2 IDH mutant). Standardized preoperative imaging (T1-, T2-, FLAIR-weighted, and T1G MRI, perfusion and diffusion MRI, MR spectroscopy and O-(2-[18F]-fluoroethyl)-L-tyrosine ([18F]FET) PET) was co-localized with multiregion stereotactic biopsies preceding resection. Tumor presence in the biopsies was assessed by 2 neuropathologists. Diagnostic accuracy was determined using receiver operating characteristic analysis.
Results. A total of 174 biopsies were obtained (63 from 9 non-enhancing and 111 from 11 enhancing gliomas), of which 129 contained tumor (50 from non-enhancing and 79 from enhancing gliomas). In enhancing gliomas, the combination of apparent diffusion coefficient (ADC) with [18F]FET PET (area under the curve [AUC], 95% CI: 0.89, 0.79–0.99) detected tumor better than T1G MRI (0.56, 0.39–0.72; $P < 0.001$) and [18F]FET PET (0.76, 0.66–0.86; $P = 0.001$). In non-enhancing gliomas, no imaging combination detected tumor significantly better than standard MRI. FLAIR-weighted MRI had an AUC of 0.81 (0.65–0.98) compared with 0.69 (0.56–0.81; $P = 0.019$) for [18F]FET PET.
Conclusion. Combining ADC and [18F]FET PET detects glioma infiltration better than standard MRI and [18F]FET PET in enhancing gliomas, potentially enabling better guidance of local therapy.

Key Points

1. Combination of ADC MRI and [18F]FET PET detects glioma infiltration better than standard MRI and [18F]FET PET in enhancing gliomas.

2. Combination of ADC MRI and [18F]FET PET may enable better image-guided surgery/ irradiation in enhancing gliomas.

Importance of the Study

Despite the suboptimal accuracy of standard MRI to detect diffuse glioma infiltration, no new imaging standard has been established, although amino acid PET has been suggested. The few prior studies suffered from limited number of imaging sequences, imprecise correlation between imaging measurements and histopathological verification, and overrepresentation of enhancing tumors. This study shows that a combination of ADC and [18F]FET PET detects glioma infiltration more accurately than standard MRI and [18F]FET PET in enhancing gliomas, as well as high-grade, IDH-wildtype, and [18F]FET positive gliomas, potentially enabling better guidance of surgery and irradiation. A future randomized controlled trial is therefore needed to compare ADC/FET and current standard MRI to guide surgery and radiotherapy.

Imaging of diffuse glioma infiltration guides decisions for initial local treatment. For instance, surgical resection aims to remove as much tumor as possible guided by standard MRI: T1-weighted gadolinium-enhanced (T1G) sequences for enhancing gliomas and T2-weighted (T2w) or fluid attenuated inversion recovery (FLAIR)–weighted sequences for non-enhancing gliomas. Furthermore, irradiation is guided by T1G MRI abnormalities with centimeter margins and FLAIR MRI abnormalities for enhancing gliomas[1] and T2w or FLAIR MRI abnormalities with centimeter margins for non-enhancing gliomas.[1,2]

Several observations challenge the accuracy of standard MRI to detect glioma infiltration: glioma cells have been detected outside MRI abnormalities,[3,4] most gliomas recur locally after gross total resection,[5,6] and survival is poor even after radiologically complete resections.[7,8] In a recent meta-analysis, amino acid PET and magnetic resonance spectroscopy (MRS) were more sensitive for glioma infiltration detection in enhancing gliomas than standard MRI.[9] Furthermore, the Response Assessment in Neuro-Oncology (RANO) working group has recently concluded amino acid PET to be superior to standard MRI for the delineation of diffuse glioma. The RANO working group, however, also suggests that combinations of imaging sequences could potentially be more accurate than single sequences.[10,11] Only a few studies have reported imaging combinations, which suffered from a limited number of imaging sequences, imprecise correlation between imaging measurements and histopathological verification, and overrepresentation of enhancing tumors.[12–18]

Better detection of glioma infiltration by imaging combinations could have several clinical benefits. First, imaging combinations should guide more extensive resections beyond the standard MRI abnormalities. The few studies that used FLAIR-weighted MRI, PET, or MRS for resections beyond standard MRI abnormalities have demonstrated longer progression-free and overall survival.[7,19–21] Second, more accurate estimation of glioma infiltration should identify patients with such extensive infiltration that partial tumor removal would be meaningless. Third, imaging combinations should improve clinical target volumes for irradiation. Finally, imaging combinations should determine tumor growth more accurately in follow-up in particular for non-enhancing gliomas.[22,23]

Diffuse gliomas can be subclassified using different biomarkers—for example, imaging markers such as enhancement on T1G MRI, histopathological markers like the World Health Organization (WHO) classification, or molecular markers such as isocitrate dehydrogenase (IDH) mutational status. Since surgical resection is mostly initiated before histopathological or molecular diagnosis, imaging markers are used to select the optimal imaging method for guidance of surgical resection.

We set out to determine the most accurate imaging combination to detect glioma infiltration in enhancing and non-enhancing gliomas using precise multiregion biopsies from regions with and without imaging abnormalities.

Methods

Study Population

The protocol of this prospective single center diagnostic study has been described elsewhere.[24] Study participants were recruited between September 2014 and June 2018 at the Brain Tumor Center of Amsterdam UMC, Netherlands. Adult patients were eligible for inclusion with an indication for resective surgery for a suspected supratentorial diffuse glioma (WHO grades II–IV), diagnosed by an experienced neuroradiologist and confirmed by the multidisciplinary neuro-oncological tumor board. Exclusion criteria were pregnancy, previous brain surgery, cranial irradiation or chemotherapy, and other brain pathology on MRI.

The study protocol was approved by the Medical Ethics Review Committee of the Free University Medical Center, and registered in the Dutch National Trial Register (NTR5354). Written informed consent was obtained from all patients.

Imaging Methods

MRI and O-(2-[18F]-fluoroethyl)-L-tyrosine ([18F]FET) PET scans were acquired within 14 days preceding surgery, both on the same day when possible. MRI was performed at 3T (Achieva, Philips Healthcare), and PET on either a Gemini TF-64 PET/CT or an Ingenuity TF PET/CT (Philips Healthcare). MRI included standard sequences: T1-weighted (T1w), T2w, FLAIR, and T1G; diffusion tensor imaging (DTI) MRI sequences yielding apparent diffusion coefficient (ADC) and fractional anisotropy (FA); perfusion MRI sequences yielding dynamic susceptibility contrast relative cerebral blood volume (DSC-CBV) and relative

cerebral blood flow (DSC-CBF) and arterial spin labeling relative cerebral blood flow (ASL-CBF), and MR spectroscopic imaging yielding Cho/NAA Index (MRSI-CNI). For [18F]FET PET, a tumor-to-brain ratio, validated with full kinetic modeling,[25] of the 20–40 minute interval was used, in accordance with European guidelines for brain tumor imaging.[26] Scan protocols, including the [18F]FET PET tumor-to-brain ratio method, are provided in the Supplementary Methods.

Multiregion Stereotactic Biopsies

All imaging sequences were linearly registered with the T1G MRI (iPlan 3.0, Brainlab) and subsequently used to plan a maximum of 12 sample locations along 3 biopsy trajectories, avoiding vascular structures and regions related with crucial functions. Preceding the craniotomy, cylindrical samples (1.8 mm diameter and 10 mm length) were obtained from regions inside and outside of imaging abnormalities using customized stereotactic procedures, detailed elsewhere,[27] to co-localize with the imaging as precise as possible (median Euclidean distance, 3.5 mm). These biopsy sample locations were digitally recorded intraoperatively to retrieve the corresponding coordinates in the imaging sequence.

Assessment of Tumor Presence

Samples were fixed in formalin, embedded in paraffin, stained with hematoxylin and eosin, and immunohistochemically analyzed with antibodies against Ki-67, p53, and R132H mutant IDH1. Two expert neuropathologists, blinded for the imaging results and patient diagnosis, independently assessed tumor presence in each sample. Consensus was obtained in case of disagreement. Histopathological diagnosis of each patient was determined from the resection material in routine procedures according to the WHO 2016 criteria.[28]

Imaging Analysis

Imaging sequence coordinates that corresponded with biopsy sample locations were used to center cubic regions of interest (ROIs) of 1 cm^3. In order to normalize the imaging sequences with relative measurements (T1w, T2w, FLAIR, T1G, DSC-CBV and -CBF, and ASL-CBF), an ROI was manually placed in the same region of the contralateral hemisphere for each biopsy location. For each imaging sequence, the mean of the voxel measurements within the biopsy and contralateral ROI were extracted for further analyses (FSL version 5.0.9, FMRIB Software Library).

Statistical Analysis

Descriptive statistics were used to report patient demographics, biopsy results, and imaging measurements of normal and tumor samples. Differences between imaging measurements of normal and tumor samples were compared using a two-sided Mann–Whitney *U*-test. Interobserver agreement between neuropathologists was measured using the kappa statistic.[29]

The optimal imaging combination in relation to tumor presence was determined in a generalized linear mixed model to remove between-subject effects. See Supplementary Methods for more details. The optimal model was determined using the Akaike information criterion.[30] The accuracy of imaging combinations to detect tumor presence was determined using receiver operating characteristic (ROC) analysis. Using the imaging measurements as a diagnostic test and the histopathological tumor presence as a reference test, the areas under the ROC curve (AUCs) with 95% confidence intervals were calculated (R package 'pROC' version 1.10.0[31]). AUCs of each single imaging method and the optimal imaging combination were compared using a nonparametric analysis of clustered binary data to account for within-patient correlation.[32] A leave-one-out cross-validation was performed to calculate prediction accuracy.

Main analysis included patients with enhancing gliomas, defined as marked contrast enhancement,[33] or non-enhancing gliomas, defined as none or mild contrast enhancement.[1] Subgroup analysis was performed for patients with high- or low-grade gliomas, defined by diagnosis according to WHO 2016 criteria,[28] IDH-wildtype or IDH-mutant gliomas, defined by immunohistochemistry for IDH1 R132H mutant protein for all but one case in which the IDH-mutant status was demonstrated by methylation profiling, and [18F]FET positive or negative gliomas, defined as tumoral uptake not exceeding background activity in visual analysis. A sensitivity analysis for non-enhancing gliomas including only patients with [18F]FET uptake was performed. Missing imaging measurements were handled by exclusion as well as by imputation.[34] The results based on these methods were similar (Supplementary Table 1). Therefore, we present the analyses with exclusion of missing imaging measurements. *P*-values less than 0.05 were considered significant. All statistical analyses were performed using R (version 3.3.2, R Foundation). The study was conducted in accordance with the Standards for Reporting of Diagnostic Accuracy Studies statement (Supplementary Table 2).[35]

Probability Map of Tumor Presence

The imaging combinations are the result of a regression analysis that used a specific formula to combine the mean values in the ROIs to predict tumor presence, so-called tumor probability, which ranges from 0 to 100%. Using this formula on the complete images, instead of only the ROIs, a tumor probability for each voxel was calculated, which resulted in a probability map of tumor presence for the whole brain. The script used to generate the ADC/FET probability map is provided in the Supplementary Material.

Results

Twenty consecutive patients were included of 51 recruited (29 did not consent and 2 withdrew after consent).

Patient characteristics are listed in Table 1. The median (interquartile range) duration between MR scan and surgery was 7 days (2–12) and between PET scan and surgery 6 days (1–11), respectively. Of the 174 biopsy samples, 111 were from the 11 enhancing gliomas and 63 from the 9 non-enhancing gliomas. Tumor was present in 129 (75%) samples, 79 (71%) samples in enhancing and 50 (79%) in non-enhancing gliomas. The number of patients, samples, and tumor presence of the subgroups are detailed in Supplementary Table 3. Exemplary images with biopsy results are presented in Fig. 1. Interobserver agreement between pathologists was moderate, with a kappa of 0.47, and higher in non-enhancing, low-grade, IDH-mutant and [18F]FET negative gliomas (kappa 0.67, 0.66, 0.61, and 0.74, respectively) than in enhancing, high-grade, IDH-wildtype and [18F]FET positive gliomas (kappa 0.39, 0.40, 0.39, and 0.44, respectively). No biopsy-related complications occurred. Visual inspection showed absence of [18F]FET PET uptake in patients 10, 15, and 16, all with a diffuse astrocytoma, IDH-mutant. Imaging measurements were missing for MRSI-CNI in 36 samples from 14 patients because of limited coverage, for [18F]FET PET in 8 samples from 1 patient because of tracer production failure, and for ASL-CBF in 2 samples of 1 patient because of image artifacts.

Imaging Measurements in Samples With and Without Tumor

In patients with enhancing glioma, imaging measurements for samples with tumor presence were significantly higher in T2w, FLAIR MRI, ADC, DSC-CBV, MRSI–CNI, and [18F]FET PET, and lower in FA, than for samples without tumor (Supplementary Figure 1A). In patients with non-enhancing glioma, imaging measurements for samples with tumor presence were significantly higher in T2w, FLAIR MRI, ADC, and [18F]FET PET, and significantly lower in T1G MRI and FA, than for samples without tumor Supplementary Figure 1B). The results of the subgroup analysis are presented in Supplementary Figure 1C–H.

Modeling and Validation of Imaging Combinations

The optimal imaging combination with the best fit in enhancing glioma was the combination of ADC with [18F]FET PET (ADC/FET), while ADC with DSC-CBF (ADC/CBF) or DSC-CBV (ADC/CBV) had the second and third best fit. In non-enhancing glioma, ADC with T1G (ADC/T1G), ADC with DSC-CBF and DSC-CBV (ADC/CBF/CBV), and T2w with T1G (T2w/T1G) had the best, second, and third best fits, respectively. Regression coefficients of these imaging combinations are detailed in Supplementary Table 4. Cross-validation prediction accuracy was highest for ADC/FET (82%) in enhancing glioma and ADC/T1G (88%) in non-enhancing glioma. Details of all imaging combinations, including cross-validation accuracy, are presented in Supplementary Table 5A, B, and for the subgroups in Supplementary Table 5C–H. The sensitivity analysis for non-enhancing gliomas including only patients with [18F]FET uptake did not result in optimal imaging combinations with [18F]FET PET.

Table 1. Patient characteristics

| Patient	Age, y	Sex	Histology	WHO Grade	IDH Status	Contrast Enhancement	Lesion Site	Biopsies, *n*
01	28	Female	Glioblastoma	IV	Mutant	Yes	Left frontal	8
02	66	Male	Glioblastoma	IV	Wildtype	Yes	Right frontal	8
03	37	Male	Astrocytoma	II	Mutant	No	Right frontal	9
04	38	Female	Glioblastoma	IV	Mutant	Yes	Left frontal	12
05	24	Male	Oligodendroglioma	II	Mutant	No	Right parietal	8
06	21	Male	Astrocytoma	II	Mutant	No	Left temporal	8
07	58	Male	Glioblastoma	IV	Wildtype	Yes	Left parietal	9
08	55	Female	Glioblastoma	IV	Wildtype	Yes	Right parietal	12
09	39	Female	Astrocytoma	II	Mutant	No	Left frontal	6
10	52	Female	Astrocytoma	II	Mutant	No	Right frontal	7
11	70	Male	Glioblastoma	IV	Wildtype	Yes	Right parietal	9
12	43	Female	Astrocytoma	II	Mutant	No	Left frontal	8
13	66	Female	Glioblastoma	IV	Wildtype	Yes	Right parietal	9
14	69	Male	Glioblastoma	IV	Wildtype	No	Left parietal	7
15	31	Male	Astrocytoma	II	Mutant	No	Left frontal	6
16	37	Male	Astrocytoma	II	Mutant	No	Left frontal	4
17	69	Male	Glioblastoma	IV	Wildtype	Yes	Right occipital	12
18	70	Female	Glioblastoma	IV	Wildtype	Yes	Right occipital	11
19	58	Male	Glioblastoma	IV	Wildtype	Yes	Right parietal	12
20	51	Male	Glioblastoma	IV	Wildtype	Yes	Left temporal	9
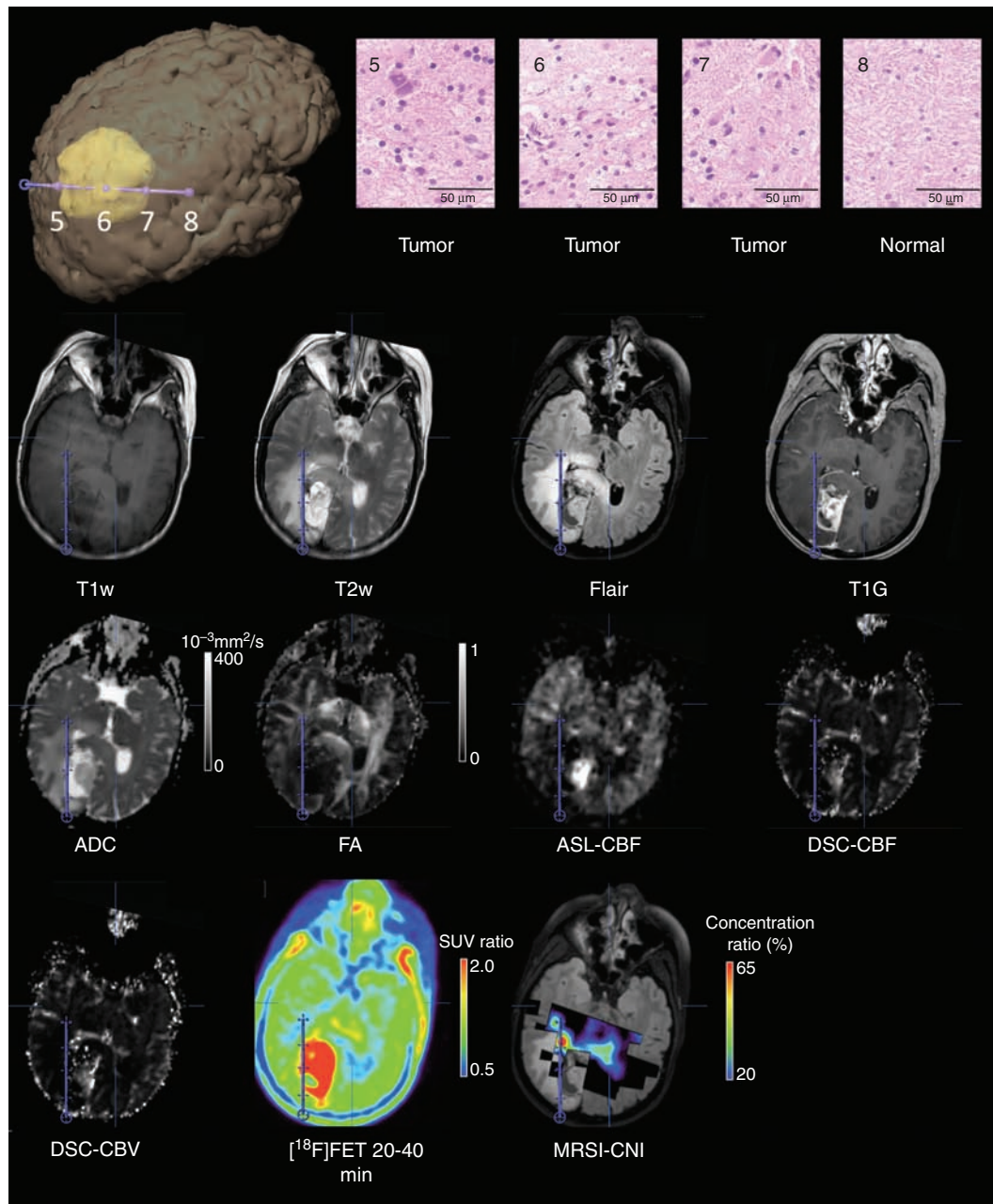
Fig. 1. Examples of imaging with corresponding histology. Example of a 55-year-old female with right occipital enhancing glioblastoma, IDH-wildtype. *First row*: on the left a 3D reconstruction of a biopsy trajectory, aimed at peripheral sample locations, with the outline of the contrast enhancement in yellow. Corresponding histology on the right. In the following rows in-line images with the trajectory and sample locations in blue. *Second row*: standard MRI, *third row*: diffusion MRI, ASL and DSC CBF and *final row*: DSC-CBV, [18F]FET PET, and MR spectroscopic imaging. Absolute imaging measurements are represented in color scales. T1w and T2w: T1- and T2-weighted MRI, FLAIR: fluid attenuation inversion recovery weighted MRI, T1G: T1-weighted gadolinium-enhanced, ADC: apparent diffusion coefficient (in 10^{-3} mm^2/s), FA: fractional anisotropy (FA), DSC-CBV and DSC-CBF: dynamic susceptibility contrast cerebral blood volume and flow, ASL-CBF: arterial spin labeling cerebral blood flow, MRSI-CNI: magnetic resonance spectroscopy imaging Cho/NAA index (concentration ratio in %), shown as overlay on FLAIR, [18F]FET: [18F]FET PET tumor-to-brain ratio 20–40 minutes interval.

Diagnostic Accuracy of Single Imaging and Imaging Combinations

The highest diagnostic accuracy in enhancing glioma was found for the ADC/FET imaging combination (AUC, 95% CI: 0.89, 0.79–0.99). In non-enhancing glioma, ADC/T1G diagnostic accuracy was highest (0.90, 0.85–0.96). In the subgroup analysis, highest accuracy in high-grade, IDH-wildtype, and [18F]FET positive glioma was found for ADC/FET (0.89, 0.80–0.99; 0.88, 0.78–0.99; and 0.90, 0.84–0.96, respectively), while

in low-grade and IDH-mutant glioma, diagnostic accuracy was highest for T2w/T1G (0.89, 0.79–0.99 and 0.91, 0.82–0.99, respectively) and in [18F]FET negative glioma, ADC/FA diagnostic accuracy was highest (1.00, 1.00–1.00). ROC plots with the AUC of each single imaging and imaging combination are provided in Supplementary Figure 2.

Comparison of Diagnostic Accuracy of Single Imaging and Imaging Combinations

In enhancing glioma, ADC/FET had a significantly higher diagnostic accuracy than each single imaging method, including T1G MRI and [18F]FET PET. ADC/CBF and ADC/CBV diagnostic accuracies were not significantly higher than ADC and [18F]FET PET. There was no significant difference in diagnostic accuracy between the imaging combinations. The diagnostic accuracy of [18F]FET PET was significantly higher than T1G MRI (Fig. 2A). In non-enhancing glioma, none of the imaging combinations' diagnostic accuracies were significantly higher than T2w or FLAIR MRI. All imaging combinations' diagnostic accuracies were higher than [18F]FET PET. The diagnostic accuracies of T2w and FLAIR MRI were almost identical. FLAIR MRI diagnostic accuracy was significantly higher than [18F]FET PET (Fig. 2B).

In the subgroup analysis of high-grade, IDH-wildtype, and [18F]FET PET positive glioma, ADC/FET diagnostic accuracy was higher than T1G MRI and [18F]FET PET, while [18F]FET PET diagnostic accuracy was higher than T1G MRI, except for in [18F]FET PET positive glioma (Fig. 2C, E, G). In low-grade and IDH-mutant glioma, T2w/T1G diagnostic accuracy was significantly higher than T2w MRI and [18F]FET PET but not FLAIR MRI. The diagnostic accuracies of T2w and FLAIR MRI were almost identical. In low-grade glioma FLAIR MRI diagnostic accuracy and in IDH-mutant glioma both T2w and FLAIR MRI diagnostic accuracies were higher than [18F]FET PET (Fig. 2D/F). In [18F]FET PET negative glioma, ADC/FA diagnostic accuracy was higher than FLAIR, but not T2w MRI (Fig. 2H); however, due to the low number of patients and samples, these results have to be interpreted with caution. Comparison of diagnostic accuracy of each single imaging and imaging combinations, including subgroup analysis, is detailed in Supplementary Table 6.

Probability Map of Tumor Presence

Probability maps for tumor presence of the ADC/FET imaging combination in enhancing gliomas were constructed. These probability maps showed larger target volumes than standard T1G MRI and [18F]FET PET in all enhancing gliomas. We observed seemingly raised tumor probability in the sulci and cisterns, which is artifactual. An exemplary probability map for tumor presence is presented in Fig. 3.

Discussion

The main finding of this prospective study is that glioma infiltration in enhancing glioma is most accurately detected by the combination of ADC and [18F]FET PET. The combination of ADC and DSC-CBF or DSC-CBV is a good alternative. This is similar in high-grade, IDH-wildtype, and [18F]FET PET positive gliomas. These imaging combinations potentially guide surgical resection and irradiation better than standard MRI and [18F]-FET PET.

The few studies that looked into imaging combinations to detect glioma infiltration all concluded that imaging combinations had a higher diagnostic accuracy than standard MRI.[12–18] Interestingly, all studies with amino acid PET, each with a majority of enhancing gliomas, included PET in their optimal imaging combination.[12–14] This is similar to our findings, although none of these studies included both amino acid PET and ADC. ADC, or mean diffusivity, was included in the optimal imaging combination of all but one study looking into diffusion imaging.[15,17,18] This could be due to the reported correlation between ADC and glioma cellularity,[36] although other studies did not find this correlation.[37] The study that did not include ADC in the optimal imaging combination aimed to identify the higher cellular tumor core, rather than tumor infiltration.[16] The use of perfusion weighted imaging (PWI) as alternative for [18F]FET PET is in line with the literature, since all studies with PWI included a perfusion metric in their optimal model.[14–16,18]

There are no studies reporting imaging combinations solemnly for non-enhancing glioma; however, one study with a majority of low-grade gliomas reported diffusion-based metrics as most accurate for discrimination between infiltration, edema, and normal tissue.[18] In our study, [18F]FET PET was not found to be a component of the optimal imaging combinations for non-enhancing glioma, and [18F]FET PET diagnostic accuracy was lower than that of FLAIR MRI, even after removing patients without [18F]FET uptake. These findings contradict the current RANO recommendations,[10] which were based on multiple studies of which 2 investigated [11C]MET or [18F]FET PET. Pauleit et al obtained 15 samples in 7 grade II glioma patients, resulting in a 100% sensitivity and 91% specificity using [18F]FET PET.[38] Since all samples were acquired from regions with abnormal MRI and/or [18F]FET PET signal, no false negative samples were obtained, in contrast to our study, explaining the higher sensitivity. Kracht et al reported a 25% underestimation of tumor extent based on 26 samples in 5 grade II astrocytoma patients, using [11C]MET PET, which is in line with our results.[39]

Both ADC/CBF and ADC/CBV could serve as alternatives for ADC/FET in enhancing gliomas, which is important in case of limited access to [18F]FET PET or limited resources. Still, we argue for the use of ADC/FET due to several reasons. First, ADC/CBF and ADC/CBF AUCs were not significantly higher than single [18F]FET PET and ADC in enhancing gliomas. Second, single DSC-CBF and DSC-CBV had lower, although not significant, diagnostic accuracies than single [18F]FET PET, which is in line with a study reporting larger tumor volumes for [18F]FET PET than DSC-CBV.[40] Finally, a recent meta-analysis found considerable heterogeneity in PWI acquisition and postprocessing.[41] This is in contrast to amino acid PET, which has European procedure guidelines.[26]

Better detection of glioma infiltration will probably result in larger target tumor volumes for surgery and
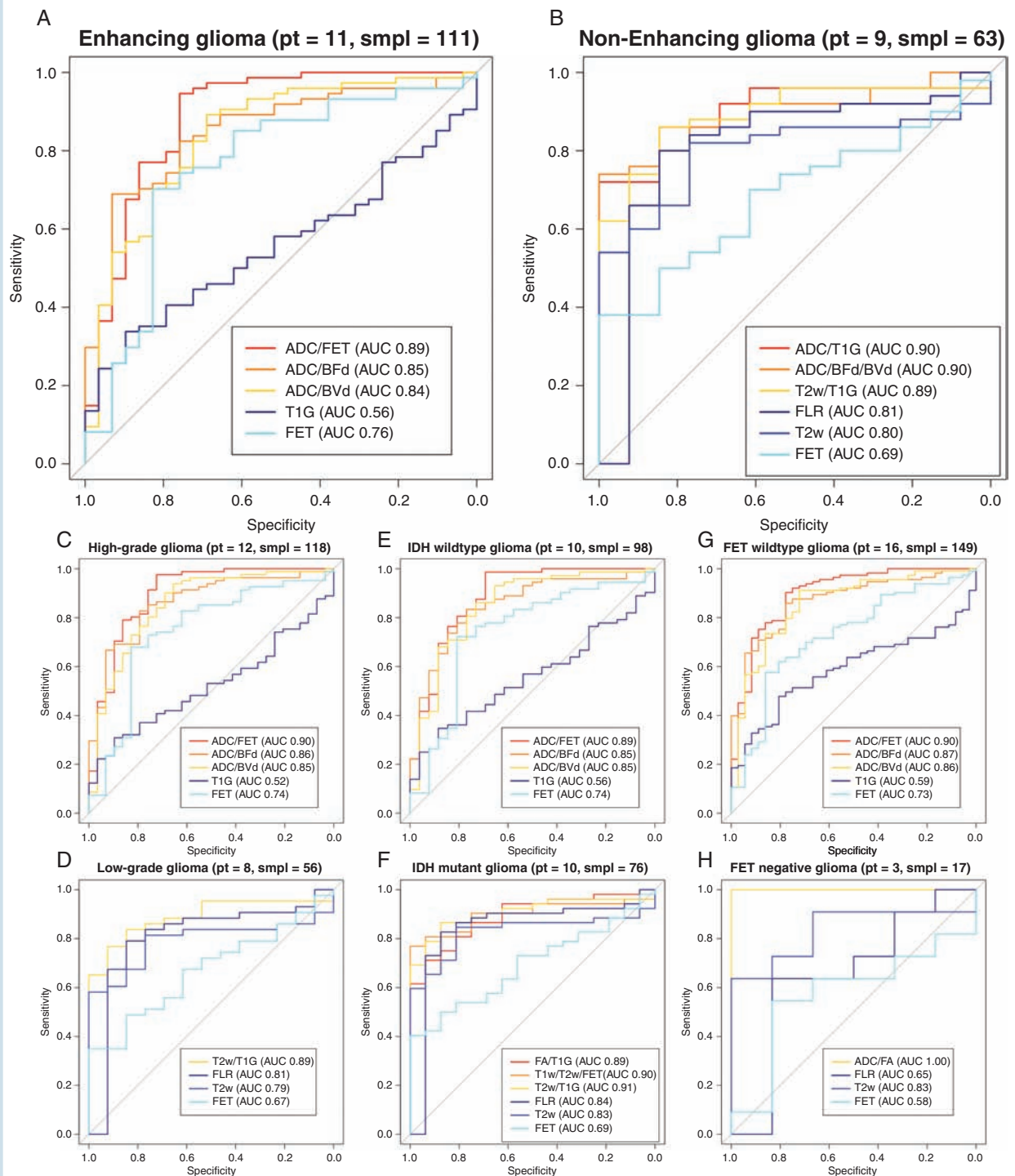
Fig. 2.   Receiver operating characteristic curves of standard MRI, [18F]FET PET, and the optimal imaging combination. ROC curves with the AUC of the optimal imaging combinations in red, orange, and yellow, standard MRI in dark and light blue, and [18F]FET PET in cyan for (A) enhancing, (B) non-enhancing, (C) high-grade, (D) low-grade, (E) IDH-wildtype, (F) IDH-mutant, (G) [18F]FET PET positive, and (H) negative glioma. The number of patients and samples of each ROC analysis is displayed in the title.

radiotherapy and may extend into critical brain structures. Therefore, considerations for the balance between maximal cytoreduction and preservation of critical brain functions are essential,[42] highlighting the need to localize critical

brain structures. In surgery, intraoperative stimulation mapping (ISM) is the standard to localize functionally critical brain structures to avoid permanent severe neurologic deficits.[43] In radiotherapy, guidelines recommend sparing
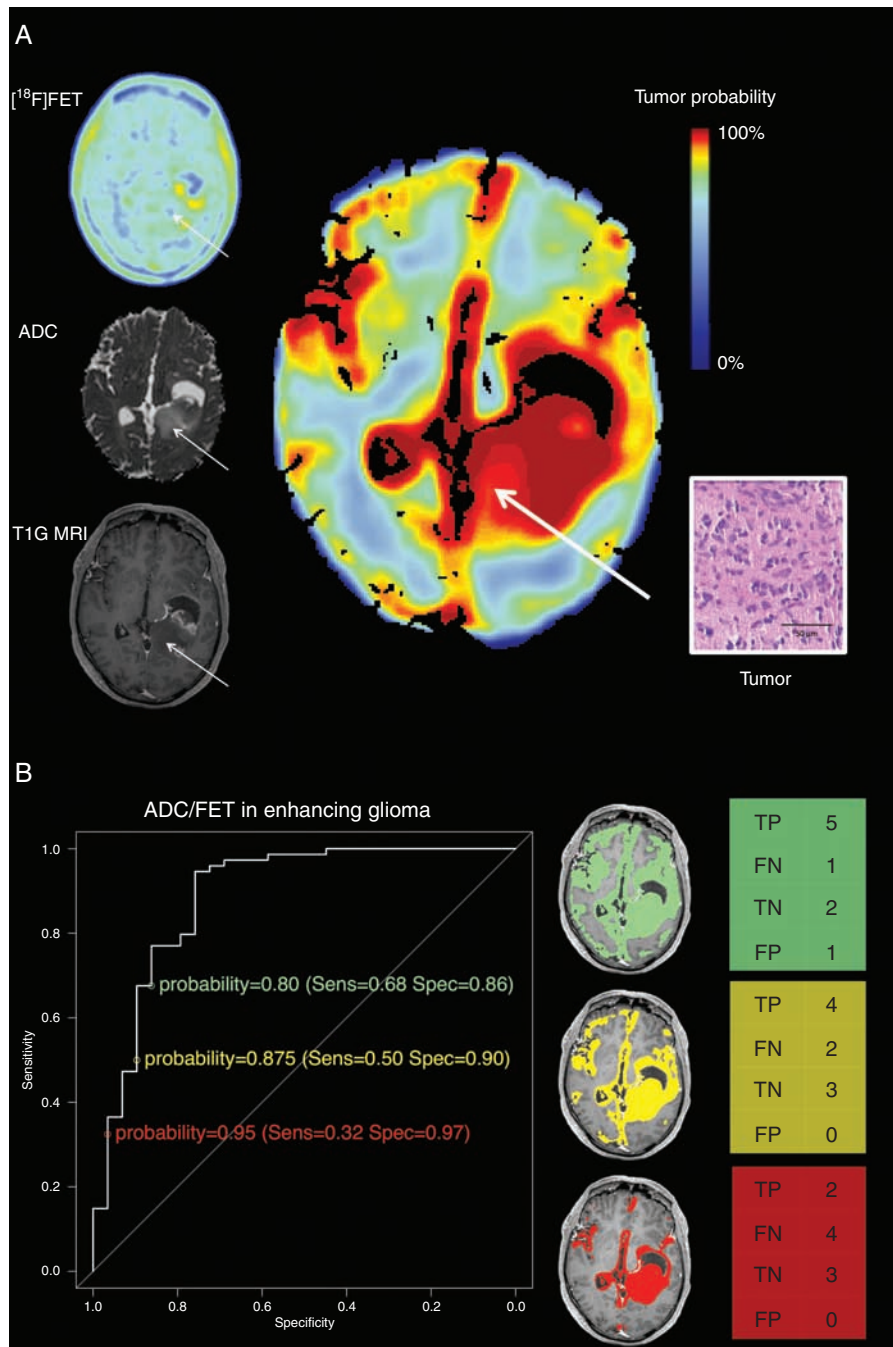
Fig. 3.   Probability map of tumor presence. (A) [18F]FET PET, ADC, T1G MRI, and a tumor probability map of the ADC/FET imaging combination for patient 20 (a 51-year-old male patient with a left central enhancing glioblastoma, IDH wildtype). The white arrows indicate a sample location with the corresponding histology on the right. Seemingly raised tumor probability in the sulci and cisterns of the probability map of tumor presence is artifactual. (B) Example of the interpretation of the ROC curve of the ADC/FET imaging combination. *Left*: ROC curve of ADC/FET imaging combination in enhancing glioma with 3 exemplary probabilities with corresponding sensitivity and specificity in green, yellow, and red. *Center*: T1G MRI with tumor delineations according to probabilities from the ROC curve for patient 20; *Right*: Tables of true positive (TP), false negative (FN), true negative (TN), and false positive (FP) samples (*n* = 9) of patient 20, according to the probabilities of the ROC curve.

of brainstem, chiasm, cochlea, eyes, lacrimal glands, lens, optical nerves, and pituitary, but so far do not recommend sparing of functionally critical cortical and subcortical brain structures.[1] A relatively new concept in radiotherapy is the use of functional MRI and DTI fiber tracking to identify critical structures and adjust target volumes.[44]

Diffuse glioma is characterized by extensive infiltration in the brain with diminishing percentages of cancer cells from

tumor core to normal brain.[4,45] This gradual cellular infiltration is notoriously difficult to detect by imaging. The ideal imaging method should quantify the fraction of glioma cells per tissue volume throughout the brain for better local treatment decisions. In essence this would provide a measure of so-called tumor purity. Tumor purity cannot even be unambiguously quantified in histological sections of samples, which were used as reference in the current study. Single cell transcriptional analysis is promising in this respect, although a limited tissue volume can be sampled.[46] Alternatively, imaging combinations can be used to calculate the probability of tumor presence for each voxel, thereby creating a probability map of tumor presence for the whole brain as shown in Fig. 3. This provides a 3D landscape of glioma cell fractions instead of current oversimplifying attempts toward binary segmentations of tumor and normal brain. This probability map of tumor presence could guide surgery and irradiation, since it allows the surgeon to select a threshold for surgical decisions and the radiation oncologist to apply dose painting planning and treatment.

The clinical benefit of local treatment guided by the combination of ADC and [18F]FET PET should be addressed in future studies—for instance, as a randomized controlled trial comparing ADC/FET and current standard imaging to guide surgery and radiotherapy in enhancing gliomas. External validation of this study could be achieved with different study designs in combination with the provided script to generate ADC/FET probability maps.

Limitations of this study include the potential for selection bias, because patients with rapid clinical progression and priority surgical scheduling were not included. Furthermore, some imaging measurements were missing for MRSI-CNI due to the restricted field of view. We selected a spatial resolution of 1 cm^3 for imaging measurements in an effort to reduce noise, but this may be lower than required for local treatment decisions. Although cross-validation demonstrated high prediction accuracies, performance in other datasets could differ from ours. We observed quite some interobserver variation between the expert neuropathologists. This can be explained by the difficulty to discern normal brain samples from samples with few glioma cells as required for this study and does not represent the accuracy of histopathological diagnosis in clinical practice. Use of immunohistochemistry for IDH1 R132H mutant protein would have introduced a bias due to the difference in assessment of IDH-wildtype and IDH-mutant gliomas. Finally, the probability maps of tumor presence have artifacts in sulci and cisterns. This is due to the high [18F]FET PET signal in large blood vessels, a known limitation of [18F]FET PET due to high blood concentration the first hour after injection[47] and high ADC signal of cerebrospinal fluid in the sulci and cisterns.

Conclusion

The imaging combination of ADC and [18F]FET PET is more accurate to detect glioma infiltration than is standard MRI in enhancing gliomas. Local treatment in enhancing gliomas by neurosurgery and radiotherapy can be optimized by guidance of this imaging combination.

Supplementary Material

Supplementary data are available at *Neuro-Oncology* online.

Keywords

brain | glioma | magnetic resonance imaging | positron-emission tomography | ROC curve

References

1. Niyazi M, Brada M, Chalmers AJ, et al. ESTRO-ACROP guideline "target delineation of glioblastomas". *Radiother Oncol.* 2016;118(1):35–42.

2. Ryken TC, Parney I, Buatti J, Kalkanis SN, Olson JJ. The role of radio-therapy in the management of patients with diffuse low grade glioma: a systematic review and evidence-based clinical practice guideline. *J Neurooncol.* 2015;125(3):551–583.

3. Kelly PJ, Daumas-Duport C, Kispert DB, Kall BA, Scheithauer BW, Illig JJ. Imaging-based stereotaxic serial biopsies in untreated intracranial glial neoplasms. *J Neurosurg.* 1987;66(6):865–874.

4. Pallud J, Varlet P, Devaux B, et al. Diffuse low-grade oligodendrogliomas extend beyond MRI-defined abnormalities. *Neurology.* 2010;74(21):1724–1731.

5. Dobelbower MC, Burnett Iii OL, Nordal RA, et al. Patterns of failure for glioblastoma multiforme following concurrent radiation and temozolomide. *J Med Imaging Radiat Oncol.* 2011;55(1):77–81.

6. McDonald MW, Shu HK, Curran WJ Jr, Crocker IR. Pattern of failure after limited margin radiotherapy and temozolomide for glioblastoma. *Int J Radiat Oncol Biol Phys.* 2011;79(1):130–136.

7. Li YM, Suki D, Hess K, Sawaya R. The influence of maximum safe resection of glioblastoma on survival in 1229 patients: can we do better than gross-total resection? *J Neurosurg.* 2016;124(4):977–988.

8. Smith JS, Chang EF, Lamborn KR, et al. Role of extent of resection in the long-term outcome of low-grade hemispheric gliomas. *J Clin Oncol.* 2008;26(8):1338–1345.

9. Verburg N, Hoefnagels FWA, Barkhof F, et al. Diagnostic accuracy of neuroimaging to delineate diffuse gliomas within the brain: a meta-analysis. *AJNR Am J Neuroradiol.* 2017;38(10):1884–1891.

10. Albert NL, Weller M, Suchorska B, et al. Response Assessment in Neuro-Oncology working group and European Association for Neuro-Oncology recommendations for the clinical use of PET imaging in gliomas. *Neuro Oncol.* 2016;18(9):1199–1208.

11. Langen KJ, Galldiks N, Hattingen E, Shah NJ. Advances in neuro-oncology imaging. *Nat Rev Neurol.* 2017;13(5):279–289.

12. Pauleit D, Floeth F, Hamacher K, et al. O-(2-[18F]fluoroethyl)-L-tyrosine PET combined with MRI improves the diagnostic assessment of cerebral gliomas. *Brain.* 2005;128(Pt 3):678–687.

13. Kinoshita M, Arita H, Goto T, et al. A novel PET index, 18F-FDG-11C-methionine uptake decoupling score, reflects glioma cell infiltration. *J Nucl Med.* 2012;53(11):1701–1708.

14. Gempt J, Soehngen E, Förster S, et al. Multimodal imaging in cerebral gliomas and its neuropathological correlation. *Eur J Radiol.* 2014;83(5):829–834.

15. Durst CR, Raghavan P, Shaffrey ME, et al. Multimodal MR imaging model to predict tumor infiltration in patients with gliomas. *Neuroradiology.* 2014;56(2):107–115.

16. Hu LS, Ning S, Eschbacher JM, et al. Multi-parametric MRI and texture analysis to visualize spatial histologic heterogeneity and tumor extent in glioblastoma. *PLoS One.* 2015;10(11):e0141506.

17. Chang PD, Malone HR, Bowden SG, et al. A multiparametric model for mapping cellularity in glioblastoma using radiographically localized biopsies. *AJNR Am J Neuroradiol.* 2017;38(5):890–898.

18. Fathi Kazerooni A, Nabil M, Zeinali Zadeh M, et al. Characterization of active and infiltrative tumorous subregions from normal tissue in brain gliomas using multiparametric MRI. *J Magn Reson Imaging.* 2018;48(4):938–950.

19. Pirotte B, Goldman S, Dewitte O, et al. Integrated positron emission tomography and magnetic resonance imaging-guided resection of brain tumors: a report of 103 consecutive procedures. *J Neurosurg.* 2006;104(2):238–253.

20. Pirotte BJ, Levivier M, Goldman S, et al. Positron emission tomography-guided volumetric resection of supratentorial high-grade gliomas: a survival analysis in 66 consecutive patients. *Neurosurgery.* 2009;64(3):471–481; discussion 481.

21. Zhang J, Zhuang DX, Yao CJ, et al. Metabolic approach for tumor delineation in glioma surgery: 3D MR spectroscopy image-guided resection. *J Neurosurg.* 2016;124(6):1585–1593.

22. Pallud J, Blonski M, Mandonnet E, et al. Velocity of tumor spontaneous expansion predicts long-term outcomes for diffuse low-grade gliomas. *Neuro Oncol.* 2013;15(5):595–606.

23. Gozé C, Blonski M, Le Maistre G, et al. Imaging growth and isocitrate dehydrogenase 1 mutation are independent predictors for diffuse low-grade gliomas. *Neuro Oncol.* 2014;16(8):1100–1109.

24. Verburg N, Pouwels PJ, Boellaard R, et al. Accurate delineation of glioma infiltration by advanced PET/MR neuro-imaging (FRONTIER Study): a diagnostic study protocol. *Neurosurgery.* 2016;79(4):535–540.

25. Koopman T, Verburg N, Schuit RC, et al. Quantification of O-(2-[18F]fluoroethyl)-L-tyrosine kinetics in glioma. *EJNMMI Res.* 2018;8(1):72.

26. Vander Borght T, Asenbaum S, Bartenstein P, et al; European Association of Nuclear Medicine (EANM). EANM procedure guidelines for brain tumour imaging using labelled amino acid analogues. *Eur J Nucl Med Mol Imaging.* 2006;33(11):1374–1380.

27. Verburg N, Baayen JC, Idema S, et al. In vivo accuracy of a frame-less stereotactic drilling technique for diagnostic biopsies and stereoelectroencephalography depth electrodes. *World Neurosurg.* 2016;87:392–398.

28. Louis DN, Perry A, Reifenberger G, et al. The 2016 World Health Organization classification of tumors of the central nervous system: a summary. *Acta Neuropathol.* 2016;131(6):803–820.

29. Cohen J. A coefficient of agreement for nominal scales. *Educational and Psychological Measurement.* 1960;20:37–46.

30. Akaike H. Information theory and an extension of the maximum likelihood principle. In: *Selected Papers of Hirotugu Akaike.* Berlin: Springer; 1998:199–213.

31. Robin X, Turck N, Hainard A, et al. pROC: an open-source package for R and S+ to analyze and compare ROC curves. *BMC Bioinformatics.* 2011;12:77.

32. Obuchowski NA. Nonparametric analysis of clustered ROC curve data. *Biometrics.* 1997;53(2):567–578.

33. Visually AcceSAble Rembrandt Images (VASARI) MRI features. Wiki for the VASARI feature set. The National Cancer Institute website. Available at: https://wiki.nci.nih.gov/display/CIP/VASARI. Accessed October 8, 2019.

34. Van Buuren S, Groothuis-Oudshoorn K. Multivariate imputation by chained equations: MICE V1.0 user's manual. *TNO Quality of Life.* 2000, PG/VGZ/00.038.

35. Bossuyt PM, Reitsma JB, Bruns DE, et al; STARD Group. STARD 2015: an updated list of essential items for reporting diagnostic accuracy studies. *BMJ.* 2015;351:h5527.

36. Surov A, Meyer HJ, Wienke A. Correlation between apparent diffusion coefficient (ADC) and cellularity is different in several tumors: a meta-analysis. *Oncotarget.* 2017;8(35):59492–59499.

37. Pauleit D, Langen KJ, Floeth F, et al. Can the apparent diffusion coefficient be used as a noninvasive parameter to distinguish tumor tissue from peritumoral tissue in cerebral gliomas? *J Magn Reson Imaging.* 2004;20(5):758–764.

38. Pauleit D, Stoffels G, Schaden W, et al. PET with O-(2-18F-fluoroethyl)-L-tyrosine in peripheral tumors: first clinical results. *J Nucl Med.* 2005;46(3):411–416.

39. Kracht LW, Miletic H, Busch S, et al. Delineation of brain tumor extent with [11C]L-methionine positron emission tomography: local comparison with stereotactic histopathology. *Clin Cancer Res.* 2004;10(21):7163–7170.

40. Filss CP, Galldiks N, Stoffels G, et al. Comparison of 18F-FET PET and perfusion-weighted MR imaging: a PET/MR imaging hybrid study in patients with brain tumors. *J Nucl Med.* 2014;55(4):540–545.

41. Patel P, Baradaran H, Delgado D, et al. MR perfusion-weighted imaging in the evaluation of high-grade gliomas after treatment: a systematic review and meta-analysis. *Neuro Oncol.* 2017;19(1):118–127.

42. Mandonnet E, Duffau H. An attempt to conceptualize the individual onco-functional balance: why a standardized treatment is an illusion for diffuse low-grade glioma patients. *Crit Rev Oncol Hematol.* 2018;122:83–91.

43. De Witt Hamer PC, Robles SG, Zwinderman AH, Duffau H, Berger MS. Impact of intraoperative stimulation brain mapping on glioma surgery outcome: a meta-analysis. *J Clin Oncol.* 2012;30(20):2559–2565.

44. Wang M, Ma H, Wang X, et al. Integration of BOLD-fMRI and DTI into radiation treatment planning for high-grade gliomas located near the primary motor cortexes and corticospinal tracts. *Radiat Oncol.* 2015;10:64.

45. Eikenberry SE, Sankar T, Preul MC, Kostelich EJ, Thalhauser CJ, Kuang Y. Virtual glioblastoma: growth, migration and treatment in a three-dimensional mathematical model. *Cell Prolif.* 2009;42(4):511–528.

46. Patel AP, Tirosh I, Trombetta JJ, et al. Single-cell RNA-seq highlights intratumoral heterogeneity in primary glioblastoma. *Science.* 2014;344(6190):1396–1401.

47. Langen KJ, Hamacher K, Weckesser M, et al. O-(2-[18F]fluoroethyl)-L-tyrosine: uptake mechanisms and clinical applications. *Nucl Med Biol.* 2006;33(3):287–294.